*Int. J. Heat Mass Transfer.* Vol. 26, No. 10, pp. 1533–1546, 1983
Printed in Great Britain

0017-9310/83 $3.00 + 0.00


# EVALUATION OF SPECTRALLY-INTEGRATED RADIATIVE FLUXES OF MOLECULAR GASES IN MULTI-DIMENSIONAL MEDIA

MICHAEL F. MODEST
Department of Mechanical Engineering, University of Southern California,
Los Angeles, CA 90007, U.S.A.

(*Received* 11 *May* 1982 *and in final form* 3 *February* 1983)

**Abstract**—A new multi-dimensional model has been developed which makes it possible to calculate the spectrally-integrated total radiative flux for a molecular-gas band based on the solution of two simple differential equations. The new model employs the exponential-wide-band model and makes it unnecessary to evaluate the spectral flux for a large number of wavenumbers with subsequent spectral integrations, thus considerably reducing the numerical effort required. Comparison with spectrally-integrated results from the differential $(P-1)$ approximation, on which the present method is based, and with some exact results, shows excellent agreement for all situations.

## NOMENCLATURE

$a$ constant in boundary condition for differential approximation, equation (3)
$b$ $a(2-\varepsilon)/\varepsilon$
$B$ boundary parameter, equation (34)
$c$ curve-fit parameter
$C_{1i}$ band strength parameter
$C_{3i}$ band width parameter
$C_2$ exponential constant in Planck function $= 1.4388$ cm K
$d$ non-dimensional distance from boundary, equation (20)
$e_b, e_{b\eta}$ (spectral) emissive power (Planck function)
$\hat{\mathbf{e}}$ unit vector in direction of flux component considered
$E_{\eta i}$ reference emissive power
$Ei, E_1, E_2, \ldots$ exponential integral functions
$f_\eta$ spacial variation function for absorption coefficient, equation (A1)
$F_1, F_2$ functions used for curve fitting
$G, H, J$ auxiliary functions, equations (39), (41) and (A5), respectively
$\hat{\mathbf{i}}, \hat{\mathbf{j}}$ unit vectors in the $\mathbf{x}(\xi)$ and $\mathbf{y}(\mu)$ directions
$I_0, I_{0\eta}$ (spectral) direction-integrated intensity
$I_0$ $I_{0\eta}$ evaluated at reference wavenumber
$K_0$ modified Bessel function
$L$ characteristic dimension
$l_\kappa$ shortest optical distance between point under consideration and a boundary, equation (18)
$\hat{\mathbf{n}}$ unit surface normal (pointing out of surface)
$\mathbf{q}, \mathbf{q}_\eta$ (spectral) radiative flux
$I_1$ first derivative of $I_{0\eta}$ with respect to spectral variation,

$$\left.\frac{\partial I_{0\eta}}{\partial \omega}\right|_{\omega(\eta_0)}$$

$q_0$ spectral flux evaluated at reference wavenumber, $\mathbf{q}_0 \cdot \hat{\mathbf{e}} = q^i_{g\eta}|_{\omega(\eta_0)}$
$q_1$ first derivative of flux with respect to spectral variation,

$$\mathbf{q}_1 \cdot \hat{\mathbf{e}} = \left.\frac{\partial q^i_{g\eta}}{\partial \omega}\right|_{\omega(\eta_0)}$$

$q^i_{g\eta}$ spectral flux within $i$th band, $\mathbf{q}^i_{g\eta} \cdot \hat{\mathbf{e}}$
$q^i_g$ total band flux, $\mathbf{q}^i_g \cdot \hat{\mathbf{e}}$
$Q_1, Q_1^*, Q_2, Q_3$ non-dimensional reference fluxes, equation (20)
$\mathbf{r}$ position vector
$T$ temperature
$u$ unity step function
$x, y$ geometric distance

Greek symbols
$\alpha$ oscillation frequency
$\varepsilon$ surface emissivity
$\kappa$ absorption coefficient
$\eta$ wavenumber
$\omega$ non-dimensional spectral decay parameter, equation (4a), (4b), (4c)
$\xi, \mu$ non-dimensional distance
$\lambda$ curve fit parameter
$\psi, \phi$ curve fit functions
$\tau$ optical thickness

Subscripts
g pertaining to gas
$i$ pertaining to $i$th gas band, or at band center (also used as superscript)
0 reference value
P Planck-mean value (of absorption coefficient)
w pertaining to wall
¢ center-line value
$\eta$ spectral value

## 1. INTRODUCTION

RADIATION from hot gases is of great importance in the design of furnaces, boilers, combustion chambers, etc.

Most previous research has focused on the simple model of a gray medium. For such a medium, multi-dimensional problems are readily solved with varying degrees of effort and accuracy. Hottel's zonal method [1, 2] has often been successfully applied, but has several shortcomings: a temperature-varying absorption coefficient complicates the analysis substantially, while scattering effects and non-gray molecular-gas effects are nearly impossible to incorporate. The multi-dimensional differential approximation [3] (often referred to as $P-1$ approximation) demands only the solution to a partial differential equation, and temperature dependent absorption coefficient as well as scattering pose no problems. However, as in Hottel's zonal method, it appears impossible to integrate the equations *a priori* over the entire spectrum, making non-gray analysis very cumbersome. The Monte Carlo method [4] has none of the above shortcomings, being readily expanded to include the most general effects. However, being a statistical method, it generally shows significant scatter in the results and demands vast amounts of computer time.

Realizing the severe shortcomings of gray-gas analyses, a number of investigators have looked at the complicated analytical treatment of non-gray molecular gas radiation in 1-dim. media. Edwards and Balakrishnan [5] formulated 1-dim. slab band absorptances for molecular gas radiation based on the exponential-wide-band model developed by Edwards and Menard [6]. They later applied this model to a turbulent gas layer [8, 9] for the cylindrical geometry. The same problem was attacked by Cess *et al.* [10] and by Tiwari and Cess [11]. Habib and Greif [12] have experimentally verified a similar analysis presented by them.

Nothing in the literature to date appears to deal with total radiative fluxes of non-gray gases in multi-dimensional media, except for some very crude approximations such as the box model by Modest [13]. This is due to the fact that, with the exception of the Monte Carlo method, spectral fluxes would have to be calculated for a large number of wavenumbers, followed by numerical integration over the entire spectrum. It is the purpose of this paper to introduce a method to predict total gas-band fluxes accurately but with a minimum of effort. This will be achieved by generating a smooth curve-fit for the spectral variation of the radiative flux, based on the diffusion approximation in the optically thick limit, and on flux as well as curve slope at an optically thin to intermediate reference wavenumber. For simplicity, the parameters for the reference wavenumber are obtained from the differential approximation, thus limiting the accuracy of the present model to that of that approximation. (For even better accuracy, variations of the zonal method could be applied at the optically thin limit.) To allow straightforward spectral integration, the popular exponential-wide-band model has been employed. (This model is known to be accurate for sufficiently high pressures, and it is assumed here that only then will molecular gas radiation be of importance. However, any other gas-band model may be employed.) Comparison of results with results obtained from wavenumber integration of the differential approximation, as well as with exact results, shows excellent agreement for all conditions tested.

The present model reduces the evaluation of total band fluxes to the solution to two differential equations and some algebraic manipulation, thus substantially reducing the efforts required by previous methods. While the method is at present limited to media without particles or other non-band emitters/absorbers, and to isothermal enclosing walls, extension to include these should be straightforward.

## 2. ANALYSIS

On a spectral basis the differential or $P-1$ approximation, relating spectral radiative flux $\mathbf{q}_\eta$ and spectral direction-integrated intensity $I_{0\eta}$ to absorption coefficient $\kappa_\eta$ and emissive power $e_{b\eta}$, has been known for a number of years, e.g. [3]

$$\nabla \cdot \mathbf{q}_\eta(\mathbf{r}) = \kappa_\eta(\mathbf{r})[4e_{b\eta}(\mathbf{r}) - I_{0\eta}(\mathbf{r})], \tag{1}$$

$$\nabla I_{0\eta}(\mathbf{r}) = -3\kappa_\eta(\mathbf{r})\mathbf{q}_\eta(\mathbf{r}), \tag{2}$$

subject to the boundary condition

$$a\mathbf{q}_\eta \cdot \hat{\mathbf{n}} = \frac{\varepsilon}{2-\varepsilon}[4e_{bw\eta} - I_{0\eta}]. \tag{3}$$

In the above equations $\hat{\mathbf{n}}$ is a unit surface normal (pointing into the medium), $\varepsilon$ is the surface emissivity (assumed gray for convenience), and $e_{bw\eta}$ is the spectral emissive power evaluated at the surface temperature and is assumed to be constant over the entire enclosure surface. The spectral variable chosen here is the wavenumber $\eta$. Since the present paper is concerned with molecular-gas radiation only, scattering terms were omitted from equations (1) and (2). Some ambiguity exists as to the value of the constant $a$ in the boundary condition. If the flux at the boundary is to be continuous, $a = 2$ (commonly known as Marshak's boundary condition) [14]. However, the use of this condition is problematic for unbounded media, as discussed by Finkleman [15], making intensity matching more desirable leading to $a = \sqrt{3}$ (known as Mark's boundary condition).

Normally, the spectral quantities are of little, if any interest. Rather, what is desired is the total radiative flux

$$\mathbf{q} = \int_0^\infty \mathbf{q}_\eta \, d\eta. \tag{4}$$

Therefore, it would be very desirable to integrate equations (1)–(3) over all wavenumbers *before* a spatial solution is obtained. However, this seems to be impossible. To date, if the differential approximation were to be used to predict thermal radiation from a molecular-gas band, equations (1)–(3) would have to be solved for many discrete wavenumbers, after which

wavenumber integration would have to be carried out by numerical quadrature. This would obviously be a very tedious process, so much so that the spectral differential approximation is usually discarded in favor of a grossly simplified model such as the box model [13], or of a purely numerical model such as the Monte Carlo method [4].

In this paper a method is presented which allows for the approximate evaluation of equation (4) in a simple fashion without the need for evaluating the spectral flux at many different wavenumbers.

We assume that the molecular gas has $N$ bands and may be described by the wide-band model, i.e.

$$\kappa_\eta = \sum_{i=1}^{N} \kappa_i(\mathbf{r}) \exp[-2|\eta-\eta_i|/C_{3i}],$$

(symmetric bands), (4a)

or

$$\kappa_\eta = \sum_{i=1}^{N} \kappa_i(\mathbf{r}) \exp[-(\eta_i-\eta)/C_{3i}], \quad \eta < \eta_i$$

(bands with head). (4b)

It is assumed here that bandwidth parameter $C_{3i}$ is constant throughout the volume. This is done for mathematical simplification, although it is realized that $C_{3i}$ generally increases with the square-root of temperature. The wide-band model is chosen for convenience, since it has been widely tabulated. This makes possible the determination of the absorption coefficient at the band center as [4]

$$\kappa_i = C_{1i}(\rho, T)/C_{3i} \tag{5}$$

where $C_{1i}$ is another wide-band parameter giving the band strength. Since $\kappa_i$ is a linear absorption coefficient, equation (5) may have to be corrected by the partial density $\rho$ or pressure of the absorbing gas, depending on the units used for $C_{1i}$. Equation (5) is strictly true only for strong-line radiation; it is assumed that only in that case is the gas radiation strong enough to be of interest.

Using the abbreviation

$$\kappa_\eta = \sum_{i=1}^{N} \kappa_i(\mathbf{r})\omega(\eta); \tag{4c}$$

and setting

$$\mathbf{q}_\eta = \sum_{i=1}^{N} \mathbf{q}^i_{g\eta}, \tag{6a}$$

$$I_{0\eta} = \sum_{i=1}^{N} I^i_{g\eta}, \tag{6b}$$

it follows that, for the $i$th band,

$$\nabla\cdot\mathbf{q}^i_{g\eta} = \kappa_i\omega(\eta)[4(e_{b\eta i}-e_{bw\eta i})-I^i_{g\eta}], \tag{7}$$

$$\nabla I^i_{g\eta} = -3\kappa_i\omega(\eta)\mathbf{q}^i_{g\eta}, \tag{8}$$

with the surface boundary condition

$$a\mathbf{q}^i_{g\eta}\cdot\hat{\mathbf{n}} + \frac{\varepsilon}{2-\varepsilon} I^i_{g\eta} = 0, \quad i = 1,2,\ldots,N. \tag{9}$$

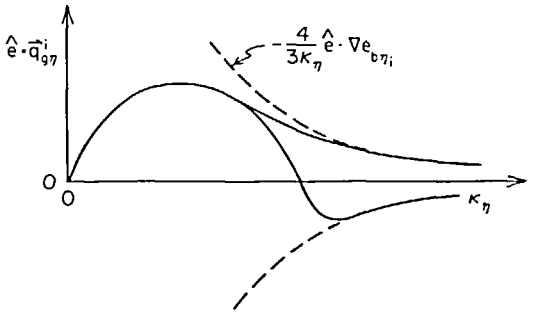


FIG. 1. Qualitative behavior of the spectral radiative flux, $q^i_{g\eta}$; as function of optical thickness.

Here the standard assumptions have been invoked that (i) the bands are narrow (i.e. $e_{b\eta}$ varies little across the bands and may be approximated by the value at the band center, $e_{b\eta i}$), and (ii) the bands do not overlap.

Looking at the qualitative behavior of the components of $\mathbf{q}^i_{g\eta}$, the flux will vary with optical thickness, and therefore with $\omega$, as is depicted in Fig. 1. At a certain optical thickness the spectral flux reaches a maximum and will decline again after further increases in optical thickness until it asymptotically reaches the value

$$\mathbf{q}^i_{g\eta} \to -\frac{4}{3\kappa_i\omega}\nabla(e_{b\eta i}-e_{bw\eta i}), \quad \kappa_i\omega L \gg 1 \tag{10}$$

where $L$ is a characteristic length of the system. If the sign of the flux at large optical thickness is opposite the one of the thin limit, the spectral flux will also go through a mimimum before approaching equation (10) (cf. Fig. 1).

It is seen from equations (7)–(9) that the spectral variation of $q^i_{g\eta}$ depends only on the parameter $\omega$, and is symmetric to the band center (for a symmetric band). Thus equation (4) may be rewritten as

$$\mathbf{q}^i_g = \int_0^\infty \mathbf{q}^i_{g\eta}(\eta)\,d\eta = t\int_0^\infty \mathbf{q}^i_{g\eta}(|\eta-\eta_i|)\,d|\eta-\eta_i|$$

$$= C_{3i}\int_0^1 \mathbf{q}^i_{g\eta}(\omega)\frac{d\omega}{\omega} \tag{11}$$

where $t = 2$ for symmetric bands, and $t = 1$ for bands with heads. The last expression in equation (11) shows that $q^i_{g\eta}/\omega$, not $q^i_{g\eta}$, is important for the evaluation of the total radiative flux. The qualitative behavior of $q^i_{g\eta}/\omega$ is depicted in Fig. 2.

In order to evaluate equation (11) accurately, an empirical fit of $q^i_{g\eta}/\omega$ should asymptotically approach the optically thick and thin limits. To assure a good fit for intermediate optical depth, one must use great care when applying the differential approximation in the optically thin limit and the diffusion approximation in the thick limit.

The differential approximation, equations (1)–(3), is known to be accurate for optically intermediate to thick situations. For isothermal walls the method will also predict the correct thin limit, i.e. heat flux rates will

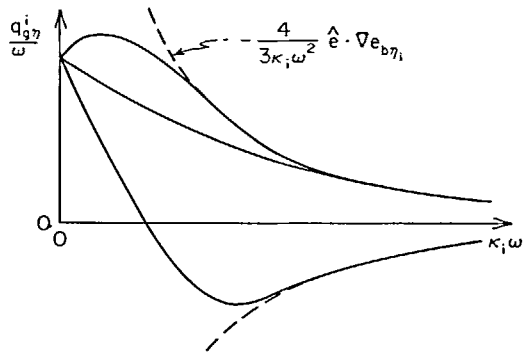


FIG. 2. Qualitative behavior of the integrand of equation (11), as function of optical thickness.

vanish as $\omega \to 0$, as long as the domain is finite. The important quantity

$$\lim_{\omega\to 0}(q^i_{g\eta}/\omega),$$

however, is very rarely predicted accurately by the differential approximation. In some cases (unbounded media) the differential approximation may predict a zero or infinite slope for $\omega \to 0$ combined with rapid changes for small $\omega$, which would lead to a poor curve fit. Even if the differential approximation is well-behaved at the thin limit, numerical evaluation of equations (7)–(9) with $\omega = 0$ would be somewhat awkward. Thus we choose to determine the value of $q^i_{g\eta}/\omega$ and of its slope at a non-zero $\omega_0 = \omega(\eta_0)$ evaluated at some reference wavenumber $\eta_0$. Expanding $q^i_{g\eta}$ into a truncated Taylor series around $\omega_0$ leads to

$$\mathbf{q}^i_{g\eta} \simeq \mathbf{q}^i_{g\eta}\Big|_{\omega_0} + (\omega-\omega_0)\frac{\partial \mathbf{q}^i_{g\eta}}{\partial\omega}\Big|_{\omega_0} + O[(\omega-\omega_0)^2]$$
$$= \mathbf{q}_0 + (\omega-\omega_0)\mathbf{q}_1 + O[(\omega-\omega_0)^2]. \quad (12)$$

If the differential approximation is well-behaved in the thin limit, the choice of $\eta_0$ will be unimportant. If it is not well-behaved at $\omega \to 0$, the choice of $\omega_0 > 0$ will assure a good fit for $\omega > \omega_0$. The values for $\mathbf{q}_0$ and $\mathbf{q}_1$ are determined from equations (7)–(9) directly or after differentiation with respect to $\omega$, respectively,

$$\nabla\cdot\mathbf{q}_0 = \kappa_i\omega_0[4(e_{b\eta i}-e_{b\omega\eta i})-I_0], \quad (13)$$
$$\nabla I_0 = -3\kappa_i\omega_0\mathbf{q}_0, \quad (14)$$

and

$$\nabla\cdot\mathbf{q}_1 = -\kappa_i\omega_0 I_1 + \kappa_i[4(e_{b\eta i}-e_{bw\eta i})-I_0], \quad (15)$$
$$\nabla I_1 = -3\kappa_i\omega_0\mathbf{q}_1 - 3\kappa_i\mathbf{q}_0, \quad (16)$$

with the boundary conditions

$$a\mathbf{q}_k\cdot\hat{\mathbf{n}} + \frac{\varepsilon}{2-\varepsilon}I_k = 0, \quad k = 0, 1. \quad (17)$$

In the optically thick limit the spectral flux will approach the diffusion limit, equation (10), everywhere except for regions close to a wall. Well inside the medium the diffusion approximation gives very accurate results even at moderate optical thickness. In order to assure a good curve-fit, it would be desirable to augment equation (10) by a boundary correction term. This may be achieved by applying the differential approximation to a region close to a flat wall leading to

$$\mathbf{q}^i_{g\eta} = -\frac{4}{3\kappa_i\omega}\nabla e_{b\eta i} - \frac{4}{b+\sqrt{3}}\Big\{(e_{b\eta i}-e_{bw\eta i})\hat{\mathbf{n}}$$
$$-\frac{1}{3\kappa_i\omega}[\sqrt{3}\nabla e_{b\eta i} + (b-\sqrt{3})\hat{\mathbf{n}}(\hat{\mathbf{n}}\cdot\nabla e_{b\eta i})]\Big\}_w$$
$$\times e^{-\sqrt{3}\omega l_\kappa} - \mathbf{R}. \quad (18)$$

In the above equation $l_\kappa$ is the optical distance from the point under consideration to the closest point at the wall (based on the absorption coefficient at the band center), $\hat{\mathbf{n}}$ is the surface normal there, $\mathbf{R}$ is some higher-order remainder, and $b$ is an abbreviation for

$$b = a\frac{2-\varepsilon}{\varepsilon}. \quad (19)$$

The subscript w at the correction term indicates that all terms inside the brackets are to be evaluated at that point on the surface. Details for the derivation of equation (18) and the remainder term $\mathbf{R}$ are shown in Appendix A.

For convenience we now introduce a number of non-dimensional quantities,

$$\tau = \kappa_i\omega L, \quad \tau_0 = \tau(\omega_0), \quad d = \sqrt{3}l_\kappa/\kappa_i L, \quad (20a)$$

$$Q_1 = -\frac{4\tau_0^2}{3\kappa_i\omega_0}\hat{e}\cdot\nabla e_{b\eta i}/\mathbf{q}_0\cdot\hat{e},$$

$$Q_1^* = -\frac{4\tau_0^2}{3\kappa_i\omega_0}[\sqrt{3}\nabla e_{b\eta i} + (b-\sqrt{3})\hat{\mathbf{n}}(\hat{\mathbf{n}}\cdot\nabla e_{b\eta i})]_w\cdot\hat{\mathbf{e}}$$
$$\div (b+\sqrt{3})\mathbf{q}_0\cdot\hat{\mathbf{e}}, \quad (20b)$$

$$Q_2 = \frac{1}{\tau_0}[1-\omega_0\mathbf{q}_1\cdot\hat{\mathbf{e}}/\mathbf{q}_0\cdot\hat{\mathbf{e}}],$$

$$Q_3 = -\frac{4\tau_0}{b+\sqrt{3}}(e_{b\eta i}-e_{bw\eta i})_w\hat{\mathbf{n}}\cdot\hat{\mathbf{e}}/\mathbf{q}_0\cdot\hat{\mathbf{e}}$$

where $L$ is some typical dimension and $\hat{\mathbf{e}}$ is a unit vector into the flux direction under consideration. In the above definitions $\tau$ represents a typical spectral optical thickness, $Q_1$ compares reference fluxes obtained from the diffusion approximation with those from the differential approximation, $Q_2$ describes the curvature of $\mathbf{q}^i_{g\eta}$ with respect to spectral variation, and $Q_3$ compares fluxes due to an emissive-power jump at the boundary with the differential approximation.

Using these quantities, a general expression for the spectral flux which satisfies equation (12) as well as equation (18) may be generated such as

$$\frac{\mathbf{q}^i_{g\eta}\cdot\hat{\mathbf{e}}}{\mathbf{q}_0\cdot\hat{\mathbf{e}}}\frac{\omega_0}{\omega} \simeq e^{-\lambda c(\tau-\tau_0)}[1-\psi(\tau_0)] + \psi(\tau) \quad (21)$$

where

$$\psi(\tau) = \frac{Q_1}{\tau^2} F_1'(c\tau) - \frac{Q_1^*}{\tau^2} e^{-d\tau} F_1'[(c-d)\tau] + \frac{Q_3}{\tau} e^{-d\tau} F_2'[(c-d)\tau], \quad (22a)$$

$$F_1(x) = [(2+x)\, e^{-x} + x - 2]u(x), \quad (22b)$$

$$F_2(x) = [e^{-x} + x - 1]u(x) = F_1(x) + F_1'(x). \quad (22c)$$

Here $u(x)$ is the unit-step function, i.e.

$$u(x) = \begin{cases} 0, & x < 0 \\ 1, & x > 0 \end{cases}, \quad (22d)$$

and primes indicate differentiation with respect to the argument. Equation (21) approaches the correct optically thick limit, equation (18), and also equation (12) for $\omega \to \omega_0$ provided the unknown correlation constants $\lambda$ and $c$ are determined from

$$\phi(c) \equiv Q_2 - c + \frac{Q_1}{\tau_0^3} F_1(c\tau_0) - \frac{Q_1^*}{\tau_0^3} e^{-d\tau_0} F_1[(c-d)\tau_0] + \frac{Q_3}{\tau_0^2} e^{-d\tau_0} F_2[(c-d)\tau_0] = -(\lambda - 1)c\phi'(c). \quad (23)$$

Since equation (23) is a single equation, one of the constants $\lambda$ and $c$ may be chosen freely, say $\lambda = 1$. In fact, the possibility of $\lambda \neq 1$ was included in equation (21) only to allow for such cases when equation (23) does not have a real positive root. If this occurs, the smoothest transition from optically thin to optically thick conditions is achieved by choosing the smallest possible value of $\lambda > 1$, leading to the additional equation

$$\phi'(c) = -(\lambda - 1)[\phi'(c) + c\phi''(c)]. \quad (24)$$

Thus whenever possible we choose $\lambda = 1$ and $c$ is a real positive root of equation (23). If there is no real positive root then equations (23) and (24) form a set of two equations in the two unknowns $\lambda$ and $c$. Evaluation of the constants $\lambda$ and $c$ is summarized in Table 1 and discussed in detail in Appendix B.

Spectral integration to obtain total gas-band flux may now be carried out. If the exponential wide band model is used to describe the absorption coefficient, equation (11) applies and may be integrated analytically leading to

$$\mathbf{q}_g^i \cdot \hat{\mathbf{e}} = \mathbf{q}_0 \cdot \hat{\mathbf{e}} \left\{ [1 - \psi(\tau_0)] \frac{e^{\lambda c\tau_0}}{\lambda c\tau_0} [1 - e^{-\lambda c\tau_g}] + \frac{Q_1}{\tau_0 \tau_g} [c\tau_g - 1 + e^{-c\tau_g}] - \frac{Q_1^*}{\tau_0 \tau_g} [(c-d)\tau_g - 1 + e^{-(c-d)\tau_g}] u(c-d) + \frac{Q_1^* d + Q_3}{\tau_0} [E_1(c\tau_g) - E_1(d\tau_g) + \ln(c/d)] u(c-d) \right\} \quad (25)$$

where $\tau_g = \tau(\omega = 1)$ is the optical depth at the band center. If a different spectral model for the absorption coefficient is chosen, equation (4) in conjunction with equation (21) may have to be integrated numerically. It should be noted that the present method is independent of the spectral model (as long as the spectral dependence is separable). It yields accurate results for the total band flux needing only the solution to two differential equations. As applied here the accuracy of the present model is limited to the accuracy of the spectral differential approximation.

Table 1. Regimes for correlation constants $c$ and $\lambda$

| | Regime | $c$ | $\lambda$ | Comments |
|---|---|---|---|---|
| I | $\phi(0) > 0$<br>$\phi'(\infty) < 0$ | root of<br>$\phi(c) = 0$ | 1 | cf. Fig. B1<br>only one positive real root exists |
| IIa | $\phi(0) > 0, \phi'(\infty) > 0$<br>$\phi(c_{min}) < 0, R^* > 0$ | root of $\phi(c) = 0$<br>$c > c_{min}$ | 1 | cf. Fig. B1<br>larger root since limit is approached from below |
| IIb | $\phi(0) > 0, \phi'(\infty) > 0$<br>$\phi(c_{min}) < 0, R^* < 0$ | root of $\phi(c) = 0$<br>$c < c_{min}$ | 1 | cf. Fig. B1<br>smaller root since limit is approached from above |
| IIc | $\phi(0) > 0, \phi'(\infty) > 0$<br>$\phi(c_{min}) > 0$ | root of<br>$\lambda - 1 = -\frac{\phi'}{(c\phi')'} = -\frac{\phi}{c\phi'} > 0$ | | cf. Fig. B2<br>for $\lambda > 1$ only one positive real root exists |
| III | $\phi(0) < 0$<br>$\phi'(\infty) > 0$ | root of $\phi(c) = 0$<br>$c > c_{min}$ | 1 | cf. Fig. B1<br>only one positive real root exists |

Note: $R^* = \mathbf{R} \cdot \hat{e}/\mathbf{q}_0 \cdot \hat{e} \gtrless 0$ limitation may be replaced by examining the regime of adjacent points; i.e. regime IIa is always bounded by regime III or IIc, while IIb is always bounded by regime I or IIc.

### 3. ILLUSTRATIVE EXAMPLES

In the following, two 1-dim. and one 2-dim. examples will be discussed in order to examine the strengths as well as the limitations and weaknesses of the proposed model. In the first example a semi-infinite medium bounded by a black plate with an emissive power spike close to the surface is investigated. This test case includes all possible regimes discussed in the previous section and also addresses other problems associated with the differential approximation, viz. an emissive power spike close to a boundary and an optically thin semi-infinite medium. However, in order to make exact wavenumber integration possible the absorption coefficient is assumed constant in this example. In the second test case a medium between parallel plates with symmetric emissive power distribution is examined. Variations of emissive power and absorption coefficient are chosen artificially to make comparison with exact solutions possible. In a final example a simple 2-dim. case is chosen of parallel gray plates separated by a gas with cosine-varying emissive power distribution.

#### 3.1. *Medium with emissive power spike*

Consider a 1-dim. medium bounded by cold black walls extending from $\xi = y/L = 0$ to $\xi \to \infty$ with an emissive power distribution of

$$e_{b\eta i} = E_{\eta i}\xi\, e^{-\xi}. \tag{26}$$

Examination of equation (26) shows that the emissive power is zero at $\xi = 0$, has a maximum at $\xi = 1$, and decays exponentially for large $\xi$. Assuming a constant absorption coefficient and using equation (20a) reduces equations (13)–(17) to

$$q_0'' - 3\tau_0^2 q_0 = 4\tau_0 E_{\eta i}(1-\xi)\, e^{-\xi}, \tag{27a}$$

$$2\tau_0 q_0(0) = q_0'(0), \tag{27b}$$

$$q_1'' - 3\tau_0^2 q_1 = 2\tau_g[3\tau_0 q_0 + 2E_{\eta i}(1-\xi)\, e^{-\xi}], \tag{28a}$$

$$2\tau_0 q_1(0) = q_1'(0) - 2\tau_g q_0(0). \tag{28b}$$

The solution to these differential equations is straightforward resulting in

$$q_0 = E_{\eta i} C_1 \left\{ \frac{1 - C_2 + 2\tau_0}{2+\sqrt{3}}\, e^{-\sqrt{3}\tau_0 \xi} - \tau_0(1 + C_2\xi)\, e^{-\xi} \right\}, \tag{29}$$

$$q_1 = E_{\eta i}\tau_g C_1 \times \left\{ \frac{2(1 - C_2 + 2\tau_0 - \tau_0 C_2^2) - \sqrt{3}C_2\tau_0(1 - C_2 + 2\tau_0)\xi}{(2+\sqrt{3})C_2\tau_0} \times e^{-\sqrt{3}\tau_0\xi} - \left(\frac{2}{C_2} - C_2 + \xi\right) e^{-\xi} \right\} \tag{30}$$

where

$$C_1 = \frac{4}{C_2(1 - 3\tau_0^2)}; \quad C_2 = \frac{1 - 3\tau_0^2}{1 + 3\tau_0^2}. \tag{31}$$

Obviously, the choice of the reference wavenumber, resulting in $\tau_0$, influences the results of $q_0$ and $q_1$ and, therefore, the values of the correlation constants $c$ and $\lambda$. On the other hand, if the spectral flux predicted by the differential approximation is well-behaved in the optically thin limit, then any reasonably small value for $\tau_0$ should result in good predictions of the total flux as calculated from equation (25). This was verified by varying $\tau_0$ between 0 and 2: If Mark's boundary condition is employed the results from equation (25) virtually coincide for all values of $\tau_0$. The same is true for Marshak's boundary condition, if the limit $\tau_0 \to 0$ is taken after the solution of equations (27) and (28) has been found. However, if the solution to the differential approximation, equations (15)–(17), is found after setting $\tau_0 = 0$, then $q_1$ becomes unbounded, corroborating Finkleman's reservations towards this boundary condition for unbounded media. Under these conditions evaluation of the total flux from equation (25) results are predicted too low (in absolute value) by approximately 50%. In all the following examples the value for the reference wavenumber has been fixed so that $\tau_0 = 0.5$, an optical thickness large enough to make results from the differential approximation meaningful, yet small enough to accurately treat the important effect of the band wings.

Figure 3 demonstrates the behavior of the non-dimensional quantities $\phi(0)$, $\phi'(\infty)$ and $\phi(c_{\min})$ which are important for the evaluation of the correlation constants $\lambda$ and $c$ (cf. Appendix B). The present example was chosen because the emissive-power spike forces the medium through all possible regimes with rapid variations of the above parameters, posing a severe test for the present method. At the bottom of the figure the range of the different regimes is indicated. As discussed in Appendix B, the distinction between regimes IIa and IIb can be found by evaluating the sign of the remainder in equation (18). However, from physical considerations and as seen in Fig. 3, regime IIa will always be adjacent to regime III and/or IIc, while IIb is always adjacent to I and/or IIc.

The heat transfer results are shown in Fig. 4. Also shown are results obtained by finding the solution to equations (7)–(9) with wavenumber as parameter, and subsequent integration over wavenumbers using numerical quadrature (labeled 'integrated differential approximation'). In order to avoid crowding of the figure, the exact solution is shown only by a few data points, and is found from the papers of Modest [16] or Edwards and Balakrishnan [5] as

$$\frac{q_g^i}{C_{3i}E_{\eta i}} = \int_0^\xi \{1 - 2E_3[\tau_g(\xi - \xi')]\} e_{b\eta i}(\xi') \frac{d\xi'}{\xi - \xi'} - \int_\xi^\infty \{1 - 2E_3[\tau_g(\xi' - \xi)]\} e_{b\eta i}(\xi') \frac{d\xi'}{\xi' - \xi}. \tag{32}$$

For the optically thick limit, $\tau_g \gg 1$, equation (32) can be evaluated analytically, resulting in (after considerable manipulation)

$$\frac{q_g^i}{C_{3i}E_{\eta i}} \simeq -1 + \xi\, e^{-\xi} Ei(\xi), \quad \tau_g \gg 1. \tag{33}$$

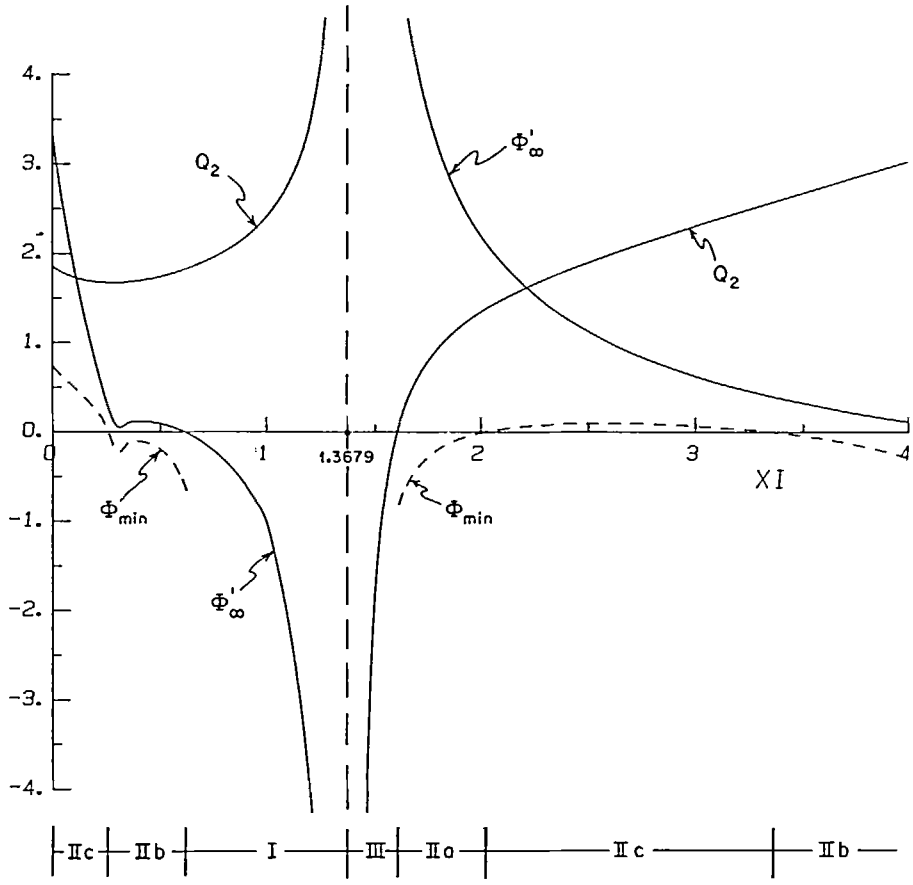


FIG. 3. Behavior of several curve-fit parameters and regime boundaries for medium with emissive power spike.

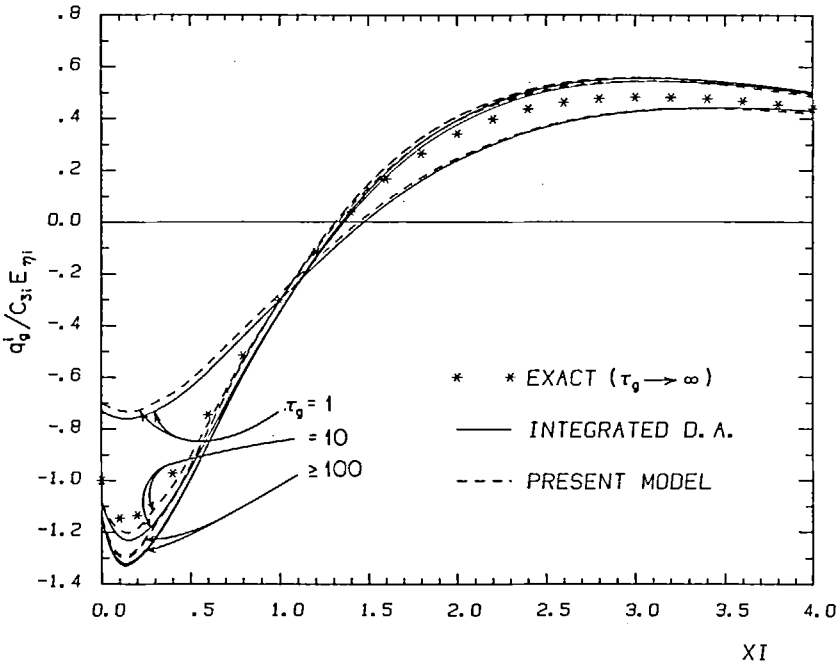


FIG. 4. Non-dimensional total band flux for semi-infinite medium with emissive power spike.

Comparison between the exact solution and the integrated differential approximation shows that the differential approximation generally overpredicts the level of heat transfer by up to about 15%, as is to be expected. The present method is generally very close to the integrated differential approximation, within about 3% of the maximum flux. The error is largest in the vicinity of the boundaries, indicating that the boundary correction is less than perfect. Errors also occur in the vicinity of the asymmetric maximum of the emissive power since equation (10) does not hold for moderate optical depths in the vicinity of such points.

3.2. *Symmetric medium with variable absorption coefficient*

Consider a 1-dim. medium $0 < \xi = y/L < 1$ with an emissive power function

$$e_{b\eta i} = E_{\eta i}\{1-\tfrac{1}{4}(2\xi-1)^2[1+(2\xi-1)^2]^2\}, \quad (34)$$

and with an absorption coefficient

$$\tau(\xi) = \kappa_i(\xi)L = \tau_m[1+3(2\xi-1)^2]. \quad (35)$$

This particular $\xi$-dependence of equations (34) and (35) was chosen because it allows a relatively simple solution of the spectral differential approximation, equations (7)–(9), and its subsequent analytical integration over wavenumbers. After considerable manipulation one gets, assuming black walls and using Mark's boundary condition ($a = \sqrt{3}$)

$$\frac{q^i_{g\eta}}{E_{\eta i}} = \frac{8}{3\tau_m\omega}\left\{x - \frac{1+\sqrt{3}\tau_m\omega}{2\sqrt{3}\tau_m\omega} \times [e^{-\sqrt{3}\tau_m\omega(1-x)} - e^{-\sqrt{3}\tau_m\omega(1+x)}]\right\}, \quad (36)$$

$$\frac{q^i_g}{C_{3i}E_{\eta i}} = \frac{8x}{2\sqrt{3}}\left(1-\frac{2}{\sqrt{3}\tau_m}\right)+\frac{2}{3\sqrt{3}\tau_m^2} \times \{[1+\sqrt{3}\tau_m(1+x)]\, e^{-(1-x)\sqrt{3}\tau_m} - [1+\sqrt{3}\tau_m(1-x)]\, e^{-(1+x)\sqrt{3}\tau_m}\} - \frac{2}{\sqrt{3}}(1-x^2)\{G[(1-x)\sqrt{3}\tau_m] - G[(1+x)\sqrt{3}\tau_m]\} \quad (37)$$

where

$$x = \tfrac{1}{2}(2\xi-1)[1+(2\xi-1)^2], \quad (38)$$

$$G(\xi) = \int_0^1 (1-e^{-\xi t})\frac{dt}{t} = E_1(\xi)+\ln\xi+\gamma, \quad (39)$$

and $\gamma = 0.5772\ldots$ is Euler's constant.

The exact solution to the present case can again be calculated by the theory given by Modest [16] and Edwards and Balakrishnan [5] so that, after some manipulation,

$$\frac{q^i_g}{C_{3i}E_{\eta i}} = \frac{2}{\tau_m^2}\{H[\tau_m(1-x)]-\tau_m H'[\tau_m(1-x)] - H[\tau_m(1+x)]+\tau_m H'[\tau_m(1+x)]\} \quad (40)$$

where

$$H(\tau) = \tfrac{2}{3}\tau+\tfrac{1}{2}\tau^2[\ln\tau+\gamma-1]+E_3(\tau)-E_5(\tau)-\tfrac{1}{4} \quad (41)$$

is the twice-integrated slab-band absorptance. For the present method, $q_0$ and $q_1$ are needed and are determined from equations (13)–(17). The solution to $q_0$, of course, is identical to $q^i_{g\eta}$ in equation (36) with $\tau_m\omega$ replaced by $\tau_0 = \tau_m\omega_0$. The solution for $q_1$ follows similarly as

$$\frac{\omega_0 q_1}{E_{\eta i}} = -\frac{8}{3\tau_0}\left\{x-\left(\frac{1}{\sqrt{3}\tau_0}+1+\tfrac{1}{2}\sqrt{3}\tau_0\right) \times [e^{-\sqrt{3}\tau_0(1-x)} - e^{-\sqrt{3}\tau_0(1+x)}] + \frac{x}{2}(1+\sqrt{3}\tau_0)[e^{-\sqrt{3}\tau_0(1-x)}+e^{-\sqrt{3}\tau_0(1+x)}]\right\}. \quad (42)$$

Again, the results for $q_0$ and $q_1$ are used to find the correlation constants $\lambda$ and $c$, after which total band fluxes are determined from equation (25). Comparison of the results is shown in Fig. 5. The wavenumber-integrated differential approximation, equation (37), generally overpredicts the heat transfer rates by approximately 20% due to errors in the optically-thin band wings. It should be noted that, in order to allow closed-form wavenumber integration of equation (36), Mark's boundary condition was used; Marshak's boundary condition would have resulted in considerably better accuracy. The accuracy of the present model as compared to the integrated differential approximation, on which it is based, is outstanding, with a maximum discrepancy of roughly 2% near the

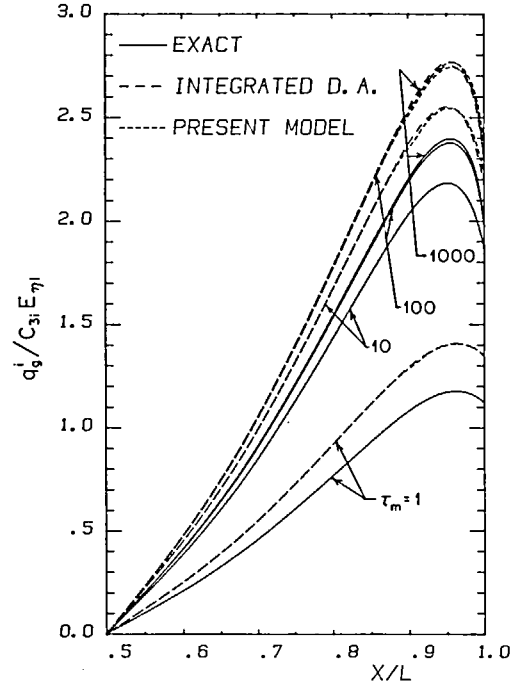


FIG. 5. Non-dimensional total band flux for finite medium with variable absorption coefficient.

boundary. Obviously, in this example, the accuracy is aided by the fact that there is no asymmetric emissive-power peak within the medium.

3.3. *Two-dimensional slab with cosine-varying emissive power*

As a final example, we consider the case of a slab $0 \leqslant \xi = y/L \leqslant 1$ with the emissive power varying in the direction parallel to the surfaces, $\mu = x/L$, according to

$$e_{b\eta i}(\mu, \xi) = E_{\eta i} \cos \alpha\mu, \tag{43}$$

with space-independent absorption coefficient and bounded by cold walls, $e_{bw\eta i} = 0$. Even though the system is 2-dim., equations (7)–(9) are readily solved because of the cosine dependence, leading to

$$\frac{\mathbf{q}^i_{g\eta} \cdot \hat{\mathbf{i}}}{E_{\eta i}} \equiv \frac{(q^i_{g\eta})_\mu}{E_{\eta i}} = \frac{\alpha\tau}{\beta^2}\left[1 - \frac{\cosh \beta(2\xi - 1)}{\cosh \beta + \dfrac{2b}{3\tau} \sinh \beta}\right] \sin \alpha\mu \tag{44}$$

$$\frac{\mathbf{q}^i_{g\eta} \cdot \hat{\mathbf{j}}}{E_{\eta i}} \equiv \frac{(q^i_{g\eta})_\xi}{E_{\eta i}} = \frac{2\tau}{\beta} \frac{\sinh \beta(2\xi - 1)}{\cosh \beta + \dfrac{2b}{3\tau} \sinh \beta} \cos \alpha\mu \tag{45}$$

where

$$\beta = \tfrac{1}{2}(\alpha^2 + 3\tau^2)^{1/2}. \tag{46}$$

In this case band integration of the spectral flux obtained above from the differential approximation cannot be achieved analytically, but is readily achieved by numerical quadrature. For a simple 2-dim. problem such as this, it is also possible to find an exact analytical expression for the band flux by first evaluating the spectral directional intensity [2, 4] as

$$I^i_{g\eta}(\mu, \xi, \hat{\mathbf{s}}) = \frac{\tau}{\pi} \int_0^{r_s(\xi, \hat{\mathbf{s}})} e_{b\eta i}[\mu_s(\mu, \hat{\mathbf{s}}, s)]\, \mathrm{e}^{-\tau_s}\, \mathrm{d}s \tag{47}$$

where $s$ is a distance non-dimensionalized by $L$ into the direction of unit vector $\hat{\mathbf{s}}$, and $r_s$ is the non-dimensional distance to the wall. Expressing direction in terms of the polar angle $\phi$ (measured from the positive $\xi$-axis) and the azimuthal angle $\psi$ (measured from the $\mu$-axis in the plane perpendicular to $\xi$), and using equation (43) results in

$$\begin{aligned} I^i_{g\eta}(\mu, \xi, \phi, \psi) &= E_{\eta i} \frac{\tau}{\pi} \int_0^{\xi} \cos\{\alpha[\mu - (\xi - \xi') \\ &\quad \times \tan \phi \cos \psi]\}\, \mathrm{e}^{-\tau(\xi - \xi')/\cos\phi} \\ &\quad \times \frac{\mathrm{d}\xi'}{\cos \phi}, \quad 0 \leqslant \phi < \frac{\pi}{2}, \\ &= E_{\eta i} \frac{\tau}{\pi} \int_{\xi}^{1} \cos\{\alpha[\mu + (\xi' - \xi) \\ &\quad \times \tan \phi \cos \psi]\}\, \mathrm{e}^{\tau(\xi' - \xi)/\cos\phi} \\ &\quad \times \frac{\mathrm{d}\xi'}{\cos \phi}, \quad \frac{\pi}{2} \leqslant \phi \leqslant \pi. \end{aligned} \tag{48}$$

From the expression for the spectral intensity the total band flux may be evaluated as

$$q^i_{g\mu} = C_{3i} \int_0^1 \int_0^{2\pi} \int_0^{\pi} I^i_{g\eta} \sin^2 \phi\, \mathrm{d}\phi \cos \psi\, \mathrm{d}\psi \frac{\mathrm{d}\omega}{\omega}, \tag{49}$$

$$q^i_{g\xi} = C_{3i} \int_0^1 \int_0^{2\pi} \int_0^{\pi} I^i_{g\eta} \cos \phi \sin \phi\, \mathrm{d}\phi\, \mathrm{d}\psi \frac{\mathrm{d}\omega}{\omega}. \tag{50}$$

After some manipulation and carrying out the spectral integration this leads to

$$\begin{aligned} \frac{q^i_{g\mu}}{C_{3i} E_{\eta i} \sin \alpha\mu} &= \frac{4}{\pi} \int_0^{\pi/2} \int_0^{\pi/2} \left\{\int_0^{\xi} + \int_0^{1-\xi}\right\} \\ &\quad \times [1 - \mathrm{e}^{-\tau_g z/\cos\phi}] \sin(\alpha z \tan \phi \cos \psi) \\ &\quad \times \frac{\mathrm{d}z}{z} \sin^2 \phi\, \mathrm{d}\phi \cos \psi\, \mathrm{d}\psi, \end{aligned} \tag{51}$$

$$\begin{aligned} \frac{q^i_{g\xi}}{C_{3i} E_{\eta i} \cos \alpha\mu} &= \frac{4}{\pi} \int_0^{\pi/2} \int_0^{\pi/2} \int_{1-\xi}^{\xi} [1 - \mathrm{e}^{-\tau_g z/\cos\phi}] \\ &\quad \times \cos(\alpha z \tan \phi \cos \psi) \frac{\mathrm{d}z}{z} \sin \phi \\ &\quad \times \cos \phi\, \mathrm{d}\phi\, \mathrm{d}\psi \end{aligned} \tag{52}$$

where the last three integrations have to be carried out numerically. However, if only the strong-band limit is needed, i.e. results for $\tau_g \to \infty$, equations (51) and (52) may be evaluated analytically leading to

$$\begin{aligned} q^i_{g\mu}(\tau_g \to \infty) &= \left[\int_0^{\alpha(1-\xi)} K_0(z)\, \mathrm{d}z \right. \\ &\quad \left. + \int_0^{\alpha\xi} K_0(z)\, \mathrm{d}z\right] C_{3i} E_{\eta i} \sin \alpha\mu, \end{aligned} \tag{53}$$

$$q^i_{g\xi}(\tau_g \to \infty) = \{K_0[\alpha(1-\xi)] - K_0[\alpha\xi]\} C_{3i} E_{\eta i} \cos \alpha\mu \tag{54}$$

where $K_0$ is the modified Bessel function, e.g. [17].

To evaluate the band fluxes by the present method, $q_0$ and $q_1$ need to be determined. Again, $q_0$ is found by setting $\tau = \tau_0$ in equations (44)–(46). $q_1$ may be found by either solving equations (15)–(17), or by differentiating equations (44) and (45) with respect to $\tau$. In either case

$$\begin{aligned} \frac{\omega_0 q_{1\mu}}{E_{\eta i} \sin \alpha\mu} &= \frac{\alpha\tau_0}{16\beta_0^4} \left\{(\alpha^2 - 3\tau_0^2)\left(\cosh \beta_0 + \frac{2b\beta_0}{3\tau_0} \right.\right. \\ &\quad \left. \times \sinh \beta_0\right)^2 + \left[3\tau_0^2\left(\left(1 + \frac{2b\beta_0^2}{3\tau_0}\right) \cosh \beta_0 \right.\right. \\ &\quad + \beta_0\left(1 + \frac{2b}{3\tau_0}\right) \sinh \beta_0\Big) \\ &\quad \left. -\alpha^2\left(\cosh \beta_0 + \frac{4b\beta_0}{3\tau_0} \sinh \beta_0\right)\right] \\ &\quad \times \cosh \beta_0(2\xi - 1) \\ &\quad -3\tau_0^2\left(\cosh \beta_0 + \frac{2b\beta_0}{3\tau_0} \sinh \beta_0\right) \\ &\quad \left. \times \beta_0(2\xi - 1) \sinh \beta_0(2\xi - 1)\right\} \\ &\quad \div \left(\cosh \beta_0 + \frac{2b\beta_0}{3\tau_0} \sinh \beta_0\right)^2, \end{aligned} \tag{55}$$

$$\frac{\omega_0 q_{1\xi}}{E_{\eta i}\cos\alpha\mu} = -\frac{\tau_0}{8\beta_0^3}\left\{\left[3\tau_0^2\beta_0\left(\sinh\beta_0+\frac{2b\beta_0}{3\tau_0}\times\cosh\beta_0\right)-\alpha^2\left(\cosh\beta_0+\frac{4b\beta_0}{3\tau_0}\sinh\beta_0\right)\right]\times\sinh\beta_0(2\xi-1)+3\tau_0^2\left(\cosh\beta_0+\frac{2b\beta_0}{3\tau_0}\sinh\beta_0\right)\times\beta_0(2\xi-1)\cosh\beta_0(2\xi-1)\right\}\div\left(\cosh\beta_0+\frac{2b\beta_0}{3\tau_0}\sinh\beta_0\right)^2. \quad (56)$$

As for the other examples, the values for $q_0$ and $q_1$ are used to form the non-dimensional parameters $Q_1$, $Q_1^*$ (which vanish for flux calculations in the $\xi$-direction), $Q_2$ and $Q_3$ (which vanishes for the $\mu$-direction), which in turn are used to determine the correlation parameters $c$ and $\lambda$ from equation (23) and the band flux from equation (25). The results using all three methods are shown in Figs. 6–11. Figure 6 shows the case of $\alpha = 0$ and $\varepsilon = 1$, i.e. a 1-dim. constant-temperature slab bounded by black walls. The exact result for this case has already been obtained by Modest [16] and follows directly from equation (52) for all optical thicknesses. As expected, the integrated differential approximation overpredicts fluxes by up to approximately 10%, in particular close to the wall with its emissive-power jump. The present model virtually coincides with the integrated differential approximation everywhere. Figures 7 and 8 show the flux across the slab for a slightly 2-dim. case of $\alpha = 0.1$, and for $\alpha = 1$. Because of the difficulty of evaluating equation (52), exact values are given only for the limiting value of $\tau_g \to \infty$ (since the wall flux is proportional to $\ln \tau_g$, no exact value is given for $\xi = 1$). The results are essentially the same as for the 1-dim. case, although, as expected, the flux diminishes somewhat with growing $\alpha$. Figure 9 shows the case of gray ($\varepsilon = 0.5$) bounding walls for $\alpha = 1$. The fluxes are essentially halved because of the reflection from the cold walls into the medium. No exact solution is readily available for this case, but it may be assumed that the differential approximation will do as well as for the black-walled case. Again, the present model shows excellent agreement.

Figures 10 and 11 show fluxes in the $\mu$-direction, i.e. parallel to the plates. For small values of $\alpha$ the differential approximation is ill-behaved in the optically-thin limit as is easily seen by examining equation (44): if one goes to the limit $\omega \to 0$ without shrinking $\alpha$, one gets

$$\lim_{\omega\to 0}\frac{(q_{g\eta}^i)_\mu}{\omega E_{\eta i}\sin\alpha\mu}\to\frac{4}{\alpha} \quad (57)$$

which blows up for small values of $\alpha$. On the other hand, if one sets $\alpha = 0$ before shrinking $\omega$, the same expression becomes identically equal to zero. Thus equation (44) has two different limits as $\alpha$ and $\omega$ approach zero. The

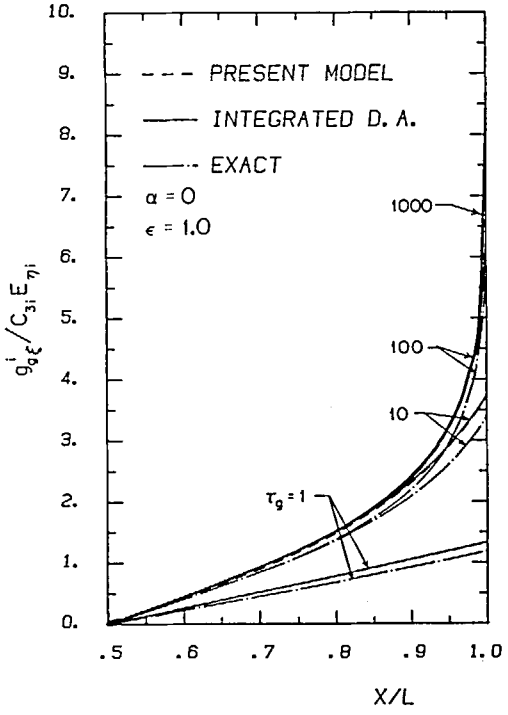


FIG. 6. Non-dimensional total band flux for one-dimensional constant-temperature slab with black walls.

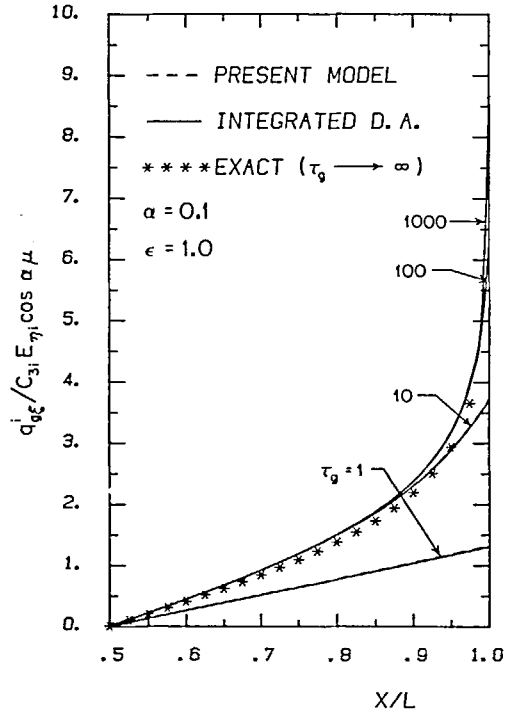


FIG. 7. Non-dimensional total band flux across slab with cosine-varying emissive power bounded by black walls ($\alpha = 0.1$).

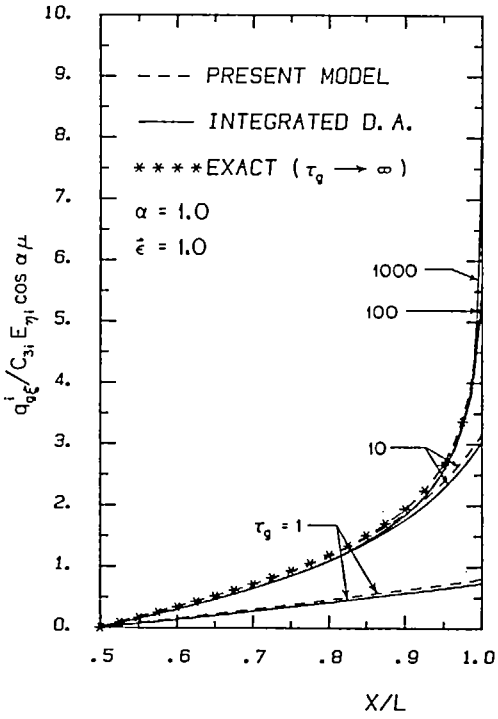


FIG. 8. Non-dimensional total band flux across slab with cosine-varying emissive power bounded by black walls ($\alpha = 1.0$).

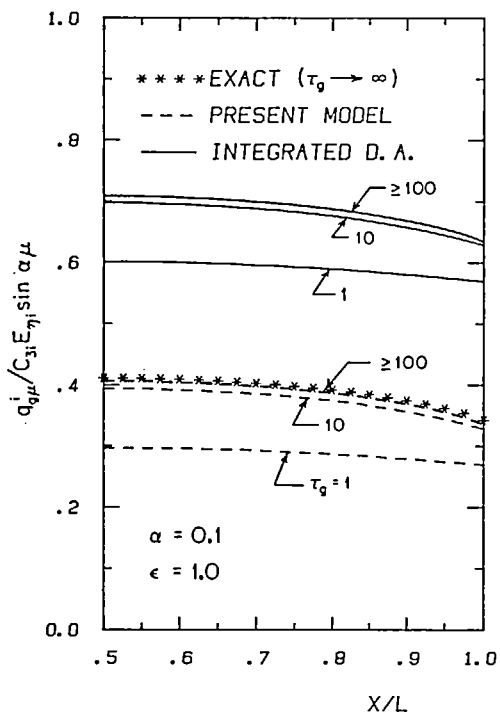


FIG. 10. Non-dimensional total band flux along slab with cosine-varying emissive power bounded by black walls ($\alpha = 0.1$).

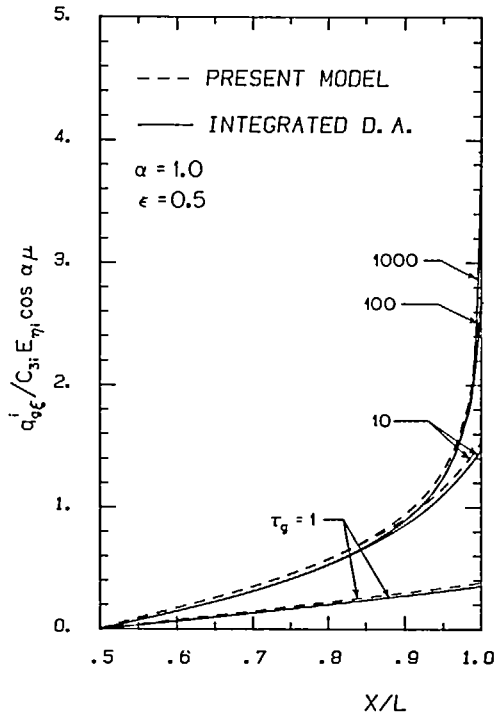


FIG. 9. Non-dimensional total band flux across slab with cosine-varying emissive power bounded by gray walls ($\varepsilon = 0.5$).

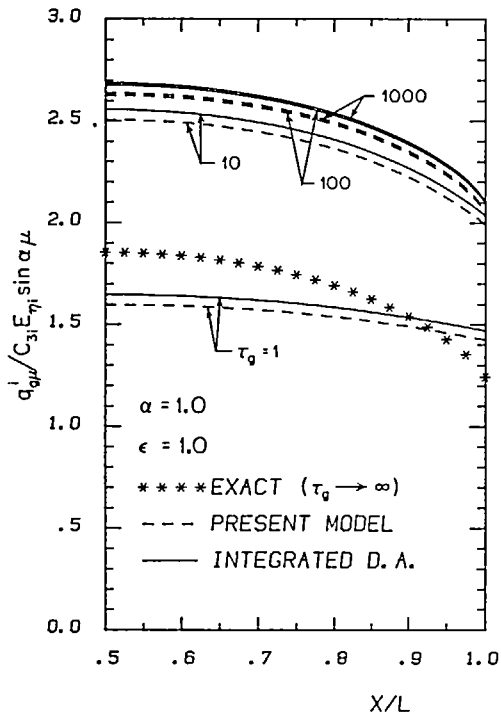


FIG. 11. Non-dimensional total band flux along slab with cosine-varying emissive power bounded by black walls ($\alpha = 1.0$).

result is that the integrated differential approximation strongly overpredicts axial fluxes for small values of $\alpha$ (Fig. 10) with slow improvement for larger values such as $\alpha = 1$ (Fig. 11). Even for relatively large values of $\alpha$ the error diminishes only slowly (approximately 20% for $\alpha = 10$). This may be explained by the infinite number of unattenuated emissive power peaks and valleys behind each point in the axial direction. For the case of $\alpha = 0.1$, the present method appears to perform exceptionally well, indeed much better than the integrated differential approximation. This is due to the fact that the choice of $\tau_0 = 0.5$ chops off the ill-behaved optically-thin limit. However, a choice of $\tau_0 < 0.5$ would have resulted in an overprediction, while a choice of $\tau_0 > 0.5$ would produce a slight underprediction of heat fluxes. Indeed, for larger values of $\alpha$ (Fig. 11) the present method and the integrated differential approximation nearly coincide again, both producing an error of roughly 50%. One may conclude that, due to its nature, the accuracy of the present method is limited by the accuracy of the integrated differential approximation.

## 4. SUMMARY

Because of the complexity of the problem, accurate multi-dimensional calculations of the total radiative flux generated by a molecular-gas vibration-rotation band have, to date, been limited to Monte Carlo evaluations. In the present paper, a model has been developed that allows the accurate prediction of the total band flux in multi-dimensional media based on the solutions to two simple differential equations (governing the optically thin limit) and on the diffusion approximation (governing the optically thick limit). As the present model is based on the differential $(P-1)$ approximation, its accuracy is limited by the accuracy of that approximation. Comparison with exact solutions shows the differential approximation generally to be within 10–15%.

Thus the present model makes it possible for the first time to calculate total radiative band fluxes from molecular gases accurately and efficiently, resulting in vast computer time savings over other accurate methods such as the Monte Carlo method. While the model is at present limited to gas mixtures without particles surrounded by isothermal surfaces, expansion of the model to allow for particle radiation and non-isothermal walls should prove fairly straightforward.

*Acknowledgement*—Partial support for this research by the National Science Foundation under Grant No. DME-8019387 is gratefully acknowledged.

## REFERENCES

1. H. C. Hottel and E. S. Cohen, Radiant heat exchange in a gas-filled enclosure: allowance for non-uniformity of gas temperature, *Trans. Am. Inst. Chem. Engrs* 4, 3–14 (1958).
2. H. C. Hottel and A. F. Sarofim, *Radiative Transfer*. McGraw-Hill, New York (1967).
3. M. F. Modest and F. H. Azad, The differential approximation for radiative transfer in an emitting, absorbing and anisotropically scattering medium, *J. Quantve Spectrosc. & Radiat. Transfer* 23, 117–120 (1980).
4. R. Siegel and J. R. Howell, *Thermal Radiation Heat Transfer* (2nd edn.). McGraw-Hill, New York (1981).
5. D. K. Edwards and A. Balakrishnan, Slab band absorptance for molecular gas radiation, *J. Quantve Spectrosc. & Radiat. Transfer* 12, 1379–1387 (1972).
6. D. K. Edwards and W. A. Menard, Comparison of models for correlation of total band absorption, *Appl. Optics* 3, 847 (1964).
7. D. K. Edwards and A. Balakrishnan, *Int. J. Heat Mass Transfer* 16, 1003 (1973).
8. A. T. Wassel and D. K. Edwards, Molecular gas band radiation in cylinders, *Trans. Am. Inst. Mech. Engrs*, Series C, *J. Heat Transfer* 96, 21–26 (1974).
9. A. T. Wassel and D. K. Edwards, Molecular gas radiation in a laminar or turbulent pipe flow, *Trans. Am. Soc. Mech. Engrs*, Series C, *J. Heat Transfer* 98, 101–107 (1976).
10. R. D. Cess, P. Mighdoll and S. N. Tiwari, Infrared radiative heat transfer in non-gray gases, *Int. J. Heat Mass Transfer* 10, 1521–1532 (1967).
11. S. N. Tiwari and R. D. Cess, Heat transfer to laminar flow of non-gray gases through a circular tube, *Appl. Scient. Res.* 25, 155–170 (1971).
12. I. S. Habib and R. Greif, Nongray radiative transport in cylindrical media, *Trans. Am. Soc. Mech. Engrs*, Series C, *J. Heat Transfer* 92, 29–32 (1970).
13. M. F. Modest, A simple differential approximation for radiative transfer in non-gray gases, *Trans. Am. Soc. Mech. Engrs*, Series C, *J. Heat Transfer* 101, 736 (1979).
14. M. F. Modest, Photon-gas formulation of the differential approximation in radiative transfer, *Lett. Heat Mass Transfer* 3, 111–116 (1976).
15. D. Finkleman, Generalized differential approximations in one-dimensional radiative transfer, *J. Quantve Spectrosc. & Radiat. Transfer* 11, 175–196 (1971).
16. M. F. Modest, Radiative heat transfer in a plane-layer mixture of non-gray particulates and molecular gases, *J. Quantve Spectrosc. & Radiat. Transfer* 26, 523–533 (1981).

## APPENDIX A
## DEVELOPMENT OF THE BOUNDARY-CORRECTION TERM

Since the diffusion approximation breaks down in the vicinity of a boundary, even for optically thick situations, equation (10) must be augmented by a boundary-correction term. If the absorption coefficient is very large, i.e. $\kappa_\eta L \gg 1$, where $L$ is some characteristic dimension, then, for a point very close to the boundary, the medium appears to be semi-infinite bounded by a plane wall. To improve on the diffusion equation one may solve the problem of a 3-dim. semi-infinite medium, employing the differential approximation and perturbation methods. To accommodate spacial variation of the absorption coefficient we let $\kappa_\eta(\mathbf{r}) = \tau f_\eta(\mathbf{r})$, where $\tau$ is a large non-dimensional constant and $f_\eta(\mathbf{r})$ is of order unity. Transforming the spacial coordinates as

$$\xi = \int_0^z f_\eta(z)\, dz, \tag{A1}$$

for the direction pointing perpendicularly into the medium, and in a similar fashion for the tangential directions, leaves to solve the equations

$$\nabla \cdot \mathbf{q}_\eta = \tau[4e_{b\eta} - I_{0\eta}], \tag{A2}$$

$$\nabla I_{0\eta} = -3\tau \mathbf{q}_\eta, \quad \tau \gg 1, \tag{A3}$$

subject to the boundary condition

$$\xi = 0: \quad b\mathbf{q}_\eta \cdot \mathbf{n} = 4e_{bw\eta} - I_{0\eta} \tag{A4}$$

where the operators are with respect to the transformed coordinates. Eliminating $q_\eta$ from equations (A2)–(A4) and setting

$$I_{0\eta}(\mathbf{r}) = J(\mathbf{r})\,e^{-\sqrt{3}\tau\xi} + 4e_{b\eta} + \frac{4}{3\tau^2}\nabla^2 e_{b\eta} + O\left\{\frac{1}{\tau^4}\right\}, \quad \text{(A5)}$$

yields a new equation for the unknown function $J$

$$\nabla^2 J - 2\sqrt{3}\tau\hat{\mathbf{n}}\cdot\nabla J = O\left\{\frac{1}{\tau^2}\right\} \quad \text{(A6)}$$

subject to

$$\xi = 0: \quad b\hat{\mathbf{n}}\cdot\nabla J - \sqrt{3}(b+\sqrt{3})\tau J = 12\tau(e_{b\eta} - e_{bw\eta}) - 4b\hat{\mathbf{n}}\cdot\nabla e_{b\eta} + \frac{4}{\tau}\nabla^2 e_{b\eta} + O\left\{\frac{1}{\tau^2}\right\}. \quad \text{(A7)}$$

Now, assuming that $\tau\xi$ is of order unity or smaller (only then is a boundary-correction term necessary), or $\xi \ll 1$, it follows from a perturbation analysis that

$$J = -\frac{4\sqrt{3}}{b+\sqrt{3}}(e_{b\eta} - e_{bw\eta})_o + \frac{1}{\tau}\frac{4b}{\sqrt{3}(b+\sqrt{3})}\hat{\mathbf{n}}\cdot(\nabla e_{b\eta})_o - \frac{1}{\tau^2}\frac{2}{b+\sqrt{3}}\left\{\nabla^2(e_{b\eta}|_o - e_{bw\eta}) \times \left(\frac{b}{\sqrt{3}(b+\sqrt{3})} + \tau\xi\right) + (\nabla^2 e_{b\eta})_o\right\} + O\left\{\frac{1}{\tau^3}\right\}, \quad \text{(A8)}$$

where the subscript o denotes evaluation at the origin at the wall. (Note that in some cases evaluation at the wall takes place before the operator is applied, and in other cases afterwards.) Therefore, using equations (A3) and (A5) the flux near a boundary may be expressed as

$$q_\eta = -\frac{4\hat{\mathbf{n}}}{b+\sqrt{3}}(e_{b\eta} - e_{bw\eta})_o\,e^{-\sqrt{3}\tau\xi} - \frac{4}{3\tau}\left\{\nabla e_{b\eta} - \frac{b}{b+\sqrt{3}}\left[\nabla(e_{b\eta} - e_{bw\eta})_o + \left(\frac{\sqrt{3}}{b} - 1\right)\nabla(e_{b\eta}|_o - e_{bw\eta})\right]e^{-\sqrt{3}\tau\xi}\right\} - \frac{4}{3\tau^2(b+\sqrt{3})}\{\mathbf{R}_1 + R_2\hat{\mathbf{n}}\}\,e^{-\sqrt{3}\tau\xi} - \frac{4}{9\tau^3}\mathbf{R}_3, \quad \text{(A9)}$$

where the $R$ are remainder terms,

$$\mathbf{R}_1 = \frac{b}{\sqrt{3}}\nabla[\hat{\mathbf{n}}\cdot(\nabla e_{b\eta})_o], \quad \text{(A10a)}$$

$$R_2 = (\nabla^2 e_{b\eta})_o + \frac{\sqrt{3}}{2}\left(\tau\xi - \frac{1}{b+\sqrt{3}}\right)\nabla^2(e_{b\eta}|_o - e_{bw\eta}), \quad \text{(A10b)}$$

$$\mathbf{R}_3 = \nabla(\nabla^2 e_{b\eta}). \quad \text{(A10c)}$$

$\mathbf{R}_1$ is a higher order term in the plane of the boundary, while $R_2$ is in the direction perpendicular to it. $R_3$ is the remainder for the diffusion approximation far away from boundaries. If equation (A1) is applied, equation (A9) reduces to equation (18) in the main body of this paper. Evaluation or estimation of the remainders is required only if the sign of $R^*$ is needed as outlined in Appendix B [cf. equation (B3)].

## APPENDIX B
## DETERMINATION OF CORRELATION CONSTANTS

In order to determine the total band flux a unique positive value for the correlation constant $c$ must be found as a root of the equation [cf. equation (23)]

$$\phi(c) = Q_2 - c + \frac{Q_1}{\tau_0^3}F_1(c\tau_0) - \frac{Q_1^*}{\tau_0^3}e^{-d\tau_0}F_1[(c-d)\tau_0] + \frac{Q_3}{\tau_0^2}e^{-d\tau_0}F_2[(c-d)\tau_0] = 0, \quad \text{(B1)}$$

Checking the second derivative of $\phi$, it is found that $\phi$ has no inflection point as long as

$$(Q_1 d + Q_3)/(Q_1 - Q_1^*) > 0. \quad \text{(B2)}$$

Far away from the boundary $e^{-d\tau} \ll 1$, and the magnitudes of $Q_1^*$ and $Q_3$ become irrelevant. Close to the boundary $|Q_1| > |Q_1^*|$, while $Q_1, Q_1^*$, and $Q_3$ may all three be expected to have the same sign from physical considerations (i.e. a temperature jump at the wall with immediate strong decline inside the medium appears physically implausible). Thus we may assume that $\phi(c)$ has no inflection points (or can be forced to have none by dropping the $Q_1^*$ and/or $Q_3$ term). This guarantees that there can be, at most, two positive real values for the constant $c$. We distinguish the following regimes (Fig. B1):

(I)
$$\phi(0) = Q_2 > 0, \quad \phi'(\infty) = -1 + \frac{Q_1}{\tau_0^2} + \frac{Q_3\tau_0 - Q_1^*}{\tau_0^2}e^{-d\tau_0} < 0;$$

(II) $\phi(0) > 0, \quad \phi'(\infty) > 0;$

(III) $\phi(0) < 0, \quad \phi'(\infty) > 0;$

A fourth possibility, i.e. when $\phi(0)$ and $\phi'(\infty)$ are negative, is discarded on physical grounds: a negative $\phi(0)$ implies that $q_{\eta}^{i}$ grows faster with optical thickness at $\tau_0$ than at the thin limit (positive curvature at $\tau_0$ in Fig. 1); a negative $\phi'(\infty)$, on the other hand, implies a switch in flux direction between the optically thin and thick limits; it is assumed, therefore, that a negative $\phi(0)$ can only be forced by a positive $\phi'(\infty)$.

It is seen from Fig. B1 that regimes I and III have one unique solution for $c$, while in regime II either zero or two roots are found, depending on whether $\phi(c_{\min})$ is positive (no root) or negative (two roots), where $c_{\min}$ is the unique root of $\phi'(c) = 0$ (cf. Fig. B1). While two roots are mathematically somewhat undesirable, that possibility is a physical necessity: if $\phi'(\infty) \ll 1$ [corresponding e.g. to a locally near-isothermal medium for which equation (18) would underpredict the flux] equation (18) should obviously be approached from the top,

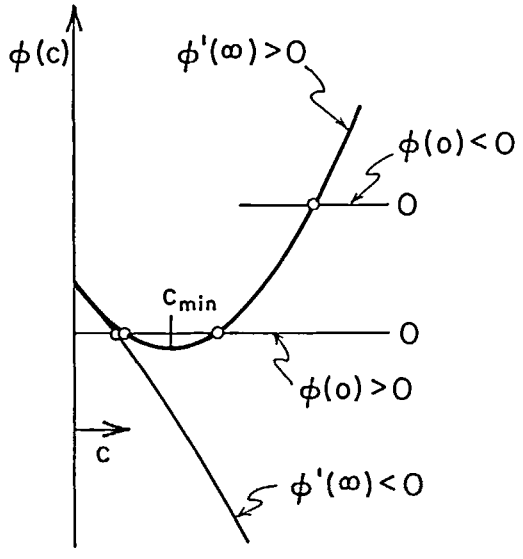


FIG. B1.

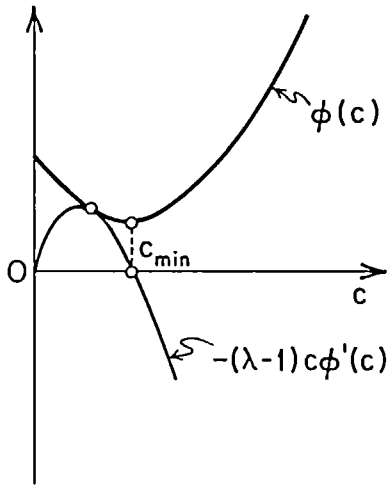


FIG. B2.

requiring $c = c_1 < c_{min}$ (regime IIb); on the other hand, if $\phi(0) \ll 1$ [corresponding to small curvature for $q^I_{sn}(\omega)$ at the optically-thin limit] equation (18) should be approached from below ($c = c_2 > c_{min}$, regime IIa). For the general case the correct root may be found by either checking adjacent points in the medium, or by determining the sign of the remainder

$$R^* = \mathbf{R} \cdot \hat{\mathbf{e}}/q_0 \cdot \hat{\mathbf{e}} \tag{B3}$$

where $\mathbf{R}$ is the remainder in equation (A10).

If $\phi(c_{min}) > 0$, equation (23) cannot be satisfied unless $\lambda \neq 1$: for $\lambda = 1$ no value for $c$ can bend the shape of the curve described by equation (21) strongly enough to obtain the high gradient desired at $\tau_0$ (described by $Q_2$). In order to overcome this problem, the spectral variation is spliced together in two parts: a low-curvature part, $\psi(\tau)$, plus an overlay which rapidly decays for positive values of $(\tau - \tau_0)$. In order to avoid implausible inflection points in equation (21) we demand a positive overlay, i.e. $\psi(\tau_0) < 1$, which necessitates $c < c_{min}$ and $\lambda > 1$. If we further postulate a minimum value for $\lambda$, to assure smoothest possible transition, equations (23) and (24) yield unique values for $\lambda$ and $c$ (cf. Fig. B2).

## EVALUATION DES FLUX RADIATIFS SPECTRALEMENT INTEGRES DES GAZ MOLECULAIRES DANS DES MILIEUX A PLUSIEURS DIMENSIONS

**Résumé**—Un nouveau modèle à plusieurs dimensions est développé pour permettre le calcul du flux radiatif total spectralement intégré pour un gaz moléculaire à bandes, à partir de deux équations différentielles simples. On emploie le modèle exponentiel à bande et il n'est pas nécessaire d'évaleur le flux spectral pour un grand nombre de nombres d'onde avec intégration spectrale, ce qui réduit l'effort numérique. Une comparaison avec des résultats spectralement intégrés à partir de l'approximation différentielle ($P-1$) sur laquelle la présente méthode est basée, et avec quelques résultats exacts, montre un excellent accord pour toutes les situations.

## BERECHNUNG DER SPEKTRAL-INTEGRIERTEN WÄRMESTRAHLUNG EINES MOLEKULAREN GASES IN EINEM MEHRDIMENSIONALEN MEDIUM

**Zusammenfassung**—Es wurde ein neues mehrdimensionales Modell entwickelt, welches die Berechnung der spektral-integrierten Gesamtstrahlung der Banden eines molekularen Gases durch die Lösung von zwei einfachen Differentialgleichungen gestattet. Das neue Modell enthält das exponentiale Breitband-Modell und macht die Berechnung der spektralen Strahlung für eine große Zahl von Wellenlängen mit nachfolgender spektraler Integration überflüssig. Auf diese Weise wird der numerische Aufwand reduziert. Ein Vergleich der spektral-integrierten Ergebnisse mit der differentiellen ($P-1$)-Approximation, auf der die beschriebene Methode beruht, mit einigen exakten Ergebnissen zeigt eine hervorragende Übereinstimmung in allen Bereichen.

## ОЦЕНКА СПЕКТРАЛЬНО УСРЕДНЕННЫХ ПОТОКОВ ИЗЛУЧЕНИЯ МОЛЕКУЛЯРНЫХ ГАЗОВ В МНОГОМЕРНЫХ СРЕДАХ

**Аннотация**—Разработана новая многомерная модель, позволяющая рассчитывать спектрально интегрированный полный поток излучения для реальной полосы молекулярного газа на основе решения двух простых дифференциальных уравнений. В новой модели используется экспоненциальная модель зоны большой ширины, что исключает необходимость проводить оценку спектрального потока для больших волновых чисел с последующим спектральным интегрированием и позволяет значительно сократить численные расчеты. Сравнение результатов, полученных с помощью дифференциального приближения ($P-1$), лежащего в основе предложенного метода, с некоторыми точными результатами дает хорошее совпадение для всех случаев.